Inorganic Chemistry
Article

Inorg. Chem. **2010**, *49*, 9891–9901 **9891**
DOI: 10.1021/ic1009253

Iridium Metal Complexes Containing N-Heterocyclic Carbene Ligands for Blue-Light-Emitting Electrochemical Cells

Cheng-Han Yang,[†,‡] Juan Beltran,[§] Vincent Lemaur,[§] Jérôme Cornil,[§] David Hartmann,[⊥] Wiebke Sarfert,[⊥] Roland Fröhlich,[¶] Claudia Bizzarri,[†,‡] and Luisa De Cola*,[†,‡]

[†]*Physikalisches Institut, Westfälische Wilhelms-Universität Münster, Mendelstrasse 7, 48149 Münster, Germany,* [‡]*Center for Nanotechnology (CeNTech), Heisenbergstrasse 11, 48149 Münster, Germany,* [§]*Service de Chimie des Matériaux Nouveaux, Université de Mons, Place du Parc 20, 7000 Mons, Belgium,* [⊥]*Siemens AG, Corporate Technology, CT MM 1, Günther-Scharowsky Strasse 1, 91058 Erlangen, Germany, and* [¶]*Organisch-Chemisches Institut, Westfälische Wilhelms-Universität Münster, Corrensstrasse 40, 48149 Münster, Germany*

Received May 9, 2010

A new series of cationic blue-emitting, heteroleptic iridium(III)-based metal complexes were systematically synthesized using two 4,6-difluorophenylpyridine ligands as well as one methyl- or *n*-butyl-substituted bisimidazolium salt carbene-type ligand. In degassed CH_2Cl_2, all complexes display highly efficient, blue phosphorescence ($\lambda_{max} \sim$ 452 nm; emission quantum yield $\sim$ 0.30) at room temperature and also show blue emission in a thin film. The measured photophysical properties of the complexes have been rationalized with the help of quantum-chemical calculations. Because of the high solubility of the complexes, solution-processed devices, light-emitting electrochemical cells (LEECs), were made. The results showed that true blue emission and short turn-on time is achieved when an ionic conductor, tetrabutylammonium trifluoromethanesulfonate, was used as the matrix for the film containing the emitters. These iridium complexes and the described devices are the bluest materials ever reported and the first case of LEECs based on carbene ligands.

Introduction

Recently, electroluminescent (EL) devices, light-emitting electrochemical cells (LEECs), based on ionic transition-metal complexes (iTMCs) have been the subject of many investigations for their simplest structure and ease manufacturing with respect to the organic light-emitting diode (OLED) preparation.[1] In such simple devices, the EL layer, which is ionic in nature, is deposited by solution-processing techniques, and because of the presence of mobile ions, which redistribute under an applied field and assist charge injection, the working mechanism of the device relies on ionic transport, differently from the OLEDs. In particular upon application of an external bias, in the LEECs, ions in the single active layer migrate and accumulate at the electrode interfaces, leading to a strong interfacial electrical field that greatly facilitates the injection of electrons and holes.[2] Most of the iTMC materials reported in the literature are based on ruthenium,[3] osmium,[4] copper,[5] and iridium[6−8] complexes,

---

*To whom correspondence should be addressed. E-mail: decola@uni-muenster.de.

(1) (a) Welter, S.; Brunner, K.; Hofstraat, J. W.; De Cola, L. *Nature* **2003**, *421*, 54. (b) Slinker, J. D.; Rivnay, J.; Moskowitz, J. S.; Parker, J. B.; Bernhard, S.; Abruna, H. D.; Malliaras, G. G. *J. Mater. Chem.* **2007**, *17*, 2976. (c) Slinker, J. D.; Bernards, D.; Houston, P. L.; Abruña, H. D.; Bernhard, S.; Malliaras, G. G. *Chem. Commun.* **2003**, 2392.

(2) Slinker, J. D.; Defranco, J. A.; Jaqutth, M. J.; Silveir, W. R.; Zhong, Y. W.; Moran-Mirabal, J. M.; Craighead, H. G.; Abruña, H. D.; Marohn, J. A.; Malliaras, G. G. *Nat. Mater.* **2007**, *6*, 894.

(3) (a) Lyons, C. H.; Abbas, E. D.; Lee, J.-K.; Rubner, M. F. *J. Am. Chem. Soc.* **1998**, *120*, 12100. (b) Gao, F. G.; Bard, A. J. *J. Am. Chem. Soc.* **2000**, *122*, 7426. (c) Buda, M.; Kalyuzhny, G.; Bard, A. J. *J. Am. Chem. Soc.* **2002**, *124*, 60908.

(4) (a) Gao, F. G.; Bard, A. J. *Chem. Mater.* **2002**, *14*, 3465. (b) Bernhard, S.; Gao, X. C.; Malliaras, G. G.; Abruña, H. D. *Adv. Mater.* **2002**, *14*, 433. (c) Hosseini, A. R.; Koh, C. Y.; Slinker, J. D.; Torres, S. F.; Abruña, H. D.; Malliaras, G. G. *Chem. Mater.* **2005**, *17*, 6114.

(5) (a) Zhang, Q. S.; Zhou, Q. G.; Cheng, Y. X.; Wang, L. X.; Ma, D. G.; Jing, X. B.; Wang, F. S. *Adv. Funct. Mater.* **2006**, *16*, 1203. (b) Armaroli, N.; Accorsi, G.; Michel, H.; Moudam, O.; Nierengarten, J. F.; Zhou, Z.; Wegh, R. T.; Welter, R. *Adv. Mater.* **2006**, *18*, 1313. (c) Zhang, Q. S.; Zhou, Q. G.; Cheng, Y. X.; Wang, L. X.; Ma, D. G.; Jing, X. B.; Wang, F. S. *Adv. Mater.* **2004**, *16*, 432. (d) Wang, Y. M.; Teng, F. Y.; Hou, B.; Xu, Z.; Wang, Y. S.; Fu, W. F. *Appl. Phys. Lett.* **2005**, *87*, 233512.

(6) (a) Slinker, J. D.; Gorodetsky, A. A.; Lowry, M. S.; Wang, J. J.; Parker, S.; Rohl, R.; Bernhard, S.; Malliaras, G. G. *J. Am. Chem. Soc.* **2004**, *126*, 2763. (b) Slinker, J. D.; Koh, C. Y.; Malliarasa, G. G.; Lowry, M. S.; Bernhard, S. *Appl. Phys. Lett.* **2005**, *86*, 173506. (c) Lowry, M. S.; Goldsmith, J. I.; Slinker, J. D.; Rohl, R.; Pascal, R. A., Jr.; Malliaras, G. G.; Bernhard, S. *Chem. Mater.* **2005**, *17*, 5712. (d) Tamayo, A. B.; Garon, S.; Sajoto, T.; Djurovich, P. I.; Tsyba, I. M.; Bau, R.; Thompson, M. E. *Inorg. Chem.* **2005**, *44*, 8723. (e) Nazeeruddin, M. K.; Wegh, R. T.; Zhou, Z.; Klein, C.; Wang, Q.; Angelis, F. D.; Fantacci, S.; Grätzel, M. *Inorg. Chem.* **2006**, *45*, 9245. (f) Bolink, H. J.; Coronado, E.; Costa, R. D.; Lardiés, N.; Ortí, E. *Inorg. Chem.* **2008**, *47*, 9149.

and typically they emit in the red, orange, yellow, green, and sky-blue regions. Among these complexes, iridium complexes are interesting candidates in terms of color tuning because of the pronounced ligand-field-splitting effects. Recently, Wong et al. and Qiu et al. reported white LEECs based on cationic iridium complexes.[9] However, reports concerning the design and preparation of blue or even near-UV ionic phosphorescent materials also based on other metal ions are relatively rare.[10]

In particular, among the iridium(III) complexes, a great number of ancillary ligands (e.g., picolate-, pyrazolylborate-, and pyridylazolate-based ligands) have been explored in order to obtain blue emission for application as OLED materials.[11] Despite a lot of effort, experimental and theoretical studies have pointed out the intrinsic difficulties in obtaining deep-blue emission because increasing the highest occupied molecular orbital (HOMO)−lowest unoccupied molecular orbital (LUMO) energy gap induces destabilization of the metal-to-ligand charge-transfer (MLCT) state and hence a decrease in the MLCT character of the lowest luminescent triplet excited state. This implies that the excited state becomes more ligand-centered, with a stronger coupling to the intramolecular vibrational modes, and that the oscillator strength of the S_0-T_1 transition as well as the emission quantum efficiency is reduced, while the radiative lifetime is increased. It has been recently reported that the use of high-field-strength ligands such as carbenes results in a shift toward higher energy of the emission and an increase of the blue phosphorescent efficiency.[12] The number of papers exploiting carbene as high-field ligand, however, remains scarce even though such ligands appear to be good candidates to achieve high-performing OLED displays, and to the best of our knowledge, no reports on LEEC devices have been published.

Herein, we report a new strategy to synthesize cationic blue-emitting, heteroleptic iridium(III)-based phosphors employing methyl- or *n*-butyl-substituted bisimidazolium salt N-heterocyclic carbene ligands as the ancillary chelate of a iridium(III) 4,6-difluorophenylpyridine complex. A full photophysical and electrochemical characterization has been performed and the experimental results compared and rationalized with quantum-chemical calculations. These complexes display deep-blue emission and high luminescent quantum yields and, because of their excellent solubility in organic solvents, have been employed as blue phosphors to fabricate blue-emitting LEECs. The emission wavelengths of the devices obtained are still very blue, the bluest ever reported for cationic species, and the LEECs possess fast turn-on time.

Experimental Section

General Information and Materials. The methyl- and *n*-butyl-substituted bisimidazolium salts (**L1** and **L2**) were prepared from the reaction of 1-methylimidazole, 1-*n*-butylimidazole, and diiodomethane in tetrahydrofuran (THF).[10b] The iridium complex $[(\mathrm{dfppy})_2\mathrm{Ir}(\mu\text{-Cl})]_2$ was synthesized using $\mathrm{IrCl_3 \cdot \mathit{n}H_2O}$ and 4,6-difluorophenylpyridine (dfppy) in 2-ethoxyethanol according to a literature method.[13] The solvents were dried using standard procedures. All other reagents were used as received from commercial sources, unless otherwise stated. NMR spectra were recorded on an ARX 300 or AMX 400 spectrometer from Bruker Analytische Messtechnik (Karlsruhe, Germany). The ^{1}H NMR chemical shifts (δ) of the signals are given in ppm and referenced to residual protons in the deuterated solvents: chloroform-d_1 (7.26 ppm), dimethyl sulfoxide-d_6 (DMSO-d_6; 2.50 ppm), or acetone-d_6 (2.09 ppm). The ^{19}F NMR chemical shifts are referenced to $\mathrm{CFCl_3}$ (0.00 ppm) as an internal standard. The signal splittings are abbreviated as follows: s = singlet; d = doublet; t = triplet; q = quartet; m = multiplet. All coupling constants (J) are given in Hertz (Hz). Mass spectrometry was performed in the Department of Chemistry, University of Münster (Münster, Germany). Electrospray ionization mass spectra were recorded on a Bruker Daltonics (Bremen, Germany) MicroTof with loop injection. Elemental analysis was recorded at the University of Milan (Milan, Italy).

Preparation of 1,1′-Dimethyl-3,3′-methylenediimidazolium Diiodide (L1). A mixture of 1-methylimidazole (12 mmol, 1.0 g, 0.97 mL) and diiodomethane (6 mmol, 1.61 g, 0.5 mL) was dissolved in 2 mL of THF in a pressure tube. The reaction mixture was stirred for 1 h at 110 °C until a white precipitate was formed. The solid was filtered off and washed with THF (5 mL) and toluene (5 mL). After that, the product was dried in vacuo and obtained as a white powder (2.31 g, 5.3 mol, 89%).

Spectra. ^{1}H NMR (300 MHz, DMSO): δ 9.40 (s, 1H), 7.99 (t, J = 1.8, 1H), 7.81 (t, J = 1.8, 1H), 6.67 (s, 1H), 3.90 (s, 3H). Anal. Calcd for $\mathrm{C_9H_{14}I_2N_4}$: C, 25.02; H, 3.27; N, 12.97. Found: C, 25.11; H, 3.32; N, 12.84.

Preparation of 1,1′-Di-*n*-butyl-3,3′-methylenediimidazolium Diiodide (L2). A mixture of 1-*n*-butylimidazole (7.6 mmol, 0.945 g, 1.0 mL) and diiodomethane (3.8 mol, 1.013 g, 0.30 mL) was dissolved in 2 mL of THF in a sealed tube. The reaction mixture was stirred for 3 h at 110 °C until a white precipitate was formed. The solid was filtered off and washed with THF (5 mL) and toluene (5 mL). After that, the product was dried in vacuo and obtained as a white powder (3.22 g, 6.2 mmol, 82%).

Spectra. ^{1}H NMR (300 MHz, DMSO): δ 9.47 (s, 1H), 8.01 (t, J = 1.7, 1H), 7.92 (t, J = 1.8, 1H), 6.64 (s, 1H), 4.23 (t, J = 7.2, 2H), 2.00−1.66 (m, 2H), 1.29 (dq, J = 7.3 and 14.6, 2H), 0.90

---

(7) (a) Bolink, H. J.; Cappelli, L.; Coronado, E.; Parham, A.; Stössel, P. *Chem. Mater.* **2006**, *18*, 2778. (b) Su, H.-C.; Wu, C.-C.; Fang, F.-C.; Wong, K.-T. *Appl. Phys. Lett.* **2006**, *89*, 261118. (c) Bolink, H. J.; Cappelli, L.; Coronado, E.; Grätzel, M.; Ortí, E.; Costa, R. D.; Viruela, P. M.; Nazeeruddin, M. K. *J. Am. Chem. Soc.* **2006**, *128*, 14786. (d) Bolink, H. J.; Coronado, E.; Costa, R. D.; Ortí, E.; Sessolo, M.; Graber, S.; Doyle, K.; Neuburger, M.; Housecroft, C. E.; Constable, E. C. *Adv. Mater.* **2008**, *20*, 3910. (e) Kwon, T. H.; Oh, Y. H.; Shin, I. S.; Hong, J. I. *Adv. Funct. Mater.* **2009**, *19*, 711.

(8) (a) Su, H.-C.; Fang, F.-C.; Hwu, T.-Y.; Hsieh, H.-H.; Chen, H.-F.; Lee, G.-H.; Peng, S.-M.; Wong, K.-T.; Wu, C.-C. *Adv. Funct. Mater.* **2007**, *17*, 1019. (b) Colman, E. Z.; Slinker, J. D.; Parker, J. B.; Malliaras, G. G.; Bernhard, S. *Chem. Mater.* **2008**, *20*, 388. (c) Graber, S.; Doyle, K.; Neuburger, M.; Housecroft, C. E.; Constable, E. C.; Costa, R. D.; Ortí, E.; Repetto, D.; Bolink, H. J. *J. Am. Chem. Soc.* **2008**, *130*, 14944.

(9) (a) Su, H.-C.; Chen, H.-F.; Fang, F.-C.; Liu, C.-C.; Wu, C.-C.; Wong, K.-T.; Liu, Y.-H.; Peng, S.-M. *J. Am. Chem. Soc.* **2008**, *130*, 3414. (b) He, L.; Qiao, J.; Duan, L.; Dong, G.; Zhang, D.; Wang, L.; Qiu, Y. *Adv. Funct. Mater.* **2009**, *19*, 2950.

(10) (a) He, L.; Duan, L.; Qiao, J.; Wang, R.; Wei, P.; Wang, L.; Qiu, Y. *Adv. Funct. Mater.* **2008**, *18*, 2123. (b) Unger, Y.; Zeller, A.; Ahrens, S.; Strassner, T. *Chem. Commun.* **2008**, 3263. (c) Lowry, M. S.; Bernhard, S. *Chem.—Eur. J.* **2006**, *12*, 7970. (d) Unger, Y.; Zeller, A.; Taige, M. A.; Strassner, T. *Dalton Trans.* **2009**, 4786.

(11) (a) Yang, C.-H.; Li, S.-W.; Chi, Y.; Cheng, Y.-M.; Yeh, Y.-S.; Chou, P.-T.; Lee, G.-H.; Wang, C.-H.; Shu, C.-F. *Inorg. Chem.* **2005**, *44*, 7770. (b) Yang, C.-H.; Cheng, Y.-M.; Chi, Y.; Hsu, C.-J.; Fang, F.-C.; Wong, K.-T.; Chou, P.-T.; Chang, C.-H.; Tsai, M.-H.; Wu, C.-C. *Angew. Chem., Int. Ed.* **2007**, *46*, 2418. (c) Sajoto, T.; Djurovich, P. I.; Tamayo, A. B.; Oxgaard, J.; Goddard, W. A.; Thompson, M. E. *J. Am. Chem. Soc.* **2008**, *131*, 9813.

(12) (a) Li, J.; Djurovich, P. I.; Alleyne, B. D.; Yousufuddin, M.; Ho, N. N.; Thomas, J. C.; Peters, J. C.; Bau, R.; Thompson, M. E. *Inorg. Chem.* **2005**, *44*, 1713. (b) Chang, C.-F.; Cheng, Y.-M.; Chi, Y.; Chiu, Y.-C.; Lin, C.-C.; Lee, G.-H.; Chou, P.-T.; Chen, C.-C; Chang, C.-H.; Wu, C.-C. *Angew. Chem., Int. Ed.* **2008**, *120*, 4618. (c) Chi, Y.; Chou, P.-T. *Chem. Soc. Rev.* **2010**, *39*, 638.

(13) Nonoyama, M. *Bull. Chem. Soc. Jpn.* **1974**, *47*, 767.

(t, J = 7.3, 3H). Anal. Calcd for $C_{15}H_{26}I_2N_4$: C, 34.90; H, 5.08; N, 10.85. Found: C, 34.72; H, 4.94; N, 10.92.

Preparation of Bis[2-(4,6-difluorophenyl)pyridinato-N,C^2]-iridium(III) [1,1′-Dimethyl-3,3′-methylenediimidazoline-2,2′-diylidene]hexafluorophosphate (1a). A mixture of 1,1′-dimethyl-3,3′-methylenediimidazolium diiodide (0.036 g, 0.083 mmol), Ag_2O (0.04 g, 0.17 mmol), and the dichloro-bridged cyclometalated iridium complex $[(dfppy)_2Ir(\mu\text{-}Cl)]_2$ (0.05 g, 0.04 mmol) in 2-ethoxyethanol (10 mL) was heated to reflux for 12 h in the dark. After cooling to room temperature, the solution was filtered through a sintered-glass frit and an excess (10 equiv) of NH_4PF_6 (in 20 mL of H_2O) was added to induce precipitation. The yellow precipitate was collected by filtration, washed with excess H_2O, and then dried under vacuum. The solid was separated using silica gel column chromatography (CH_2Cl_2: MeCN = 9:1), giving a light-yellow complex **1a** (0.052 g, 0.058 mmol, 72% yield).

Spectra. ^{1}H NMR (300 MHz, acetone): δ 8.55 (dd, J=0.8 and 5.9, 1H), 8.41 (d, J = 8.6, 1H), 8.10 (ddd, J = 0.5, 4.5, and 8.3, 1H), 7.56 (d, J = 1.9, 1H), 7.30 (ddd, J = 1.4, 5.9, and 7.3, 1H), 7.25 (d, J = 1.9, 1H), 6.58 (ddd, J = 2.4, 9.2, and 12.9, 1H), 6.39 (s, 1H), 5.92 (dd, J = 2.4 and 8.5, 1H), 3.01 (s, 3H). $^{19}F\{^1H\}$ NMR (282 MHz, acetone): δ −71.25 (3F), −73.75 (3F), −109.68 (2F), −110.48 (2F). ^{13}C NMR (101 MHz, DMSO): δ 168.36, 164.50, 163.22, 162.18, 160.72, 159.76, 159.47, 153.72, 138.87, 127.95, 124.30, 123.19, 121.95, 112.77, 97.86, 61.63, 36.47. HRMS. Found: m/z 749.1613 ($[M - PF_6]^+$). Anal. Calcd for $C_{31}H_{24}F_{10}IrN_6P$: C, 41.66; H, 2.71; N, 9.40. Found: C, 41.53; H, 2.84;N, 9.46.

Preparation of Bis[2-(4,6-difluorophenyl)pyridinato-N,C^2]-iridium(III) [1,1′-Dimethyl-3,3′-methylenediimidazoline-2,2′-diylidene]tetrafluoroborate (1b). A mixture of 1,1′-dimethyl-3,3′-methylenediimidazolium diiodide (0.36 g, 0.83 mmol), Ag_2O (0.4 g, 1.7 mmol), and the dichloro-bridged cyclometalated iridium complex $[(dfppy)_2Ir(\mu\text{-}Cl)]_2$ (0.5 g, 0.4 mmol) in 2-ethoxyethanol (20 mL) was heated to reflux for 12 h in the dark. After cooling to room temperature, the solution was then filtered through a sintered-glass frit and an excess (10 equiv) of $NaBF_4$ (in 40 mL of H_2O) was added to induce precipitation. The yellow precipitate was collected by filtration, washed with H_2O, and then dried under vacuum. The solid was separated using silica gel column chromatography (CH_2Cl_2:MeCN = 9:1), giving a light-yellow complex **1b** (0.46 g, 0.56 mmol, 68% yield).

Spectra. ^{1}H NMR (300 MHz, acetone): δ 8.60−8.51 (m, 1H), 8.46−8.35 (m, 1H), 8.16−8.03 (m, 1H), 7.58 (d, J = 2.0, 1H), 7.31 (ddd, J = 1.4, 5.9, and 7.4, 1H), 7.23 (d, J = 2.0, 1H), 6.57 (ddd, J = 2.4, 9.2, and 12.9, 1H), 6.38 (s, 1H), 5.92 (dd, J = 2.4 and 8.5, 1H), 3.00 (s, 3H). $^{19}F\{^1H\}$ NMR (282 MHz, acetone): δ −109.80 (2F), −110.52 (2F), −151.06 (4F). ^{13}C NMR (101 MHz, DMSO): δ 168.29, 164.42, 163.19, 162.14, 160.62, 159.64, 159.15, 153.66, 138.91, 128.16, 124.18, 123.20, 121.94, 112.57, 97.78, 61.64, 36.63. HRMS. Found: m/z 749.1635 ($[M - BF_4]^+$). Anal. Calcd for $C_{31}H_{24}BF_8IrN_6$: C, 44.56; H, 2.90; N, 10.06. Found: C, 44.09; H, 2.92; N, 9.84.

Preparation of Bis[2-(4,6-difluorophenyl)pyridinato-N,C^2]-iridium(III) [1,1′-Di-*n*-butyl-3,3′-methylenediimidazoline-2,2′-diylidene]hexafluorophosphate (2a). A mixture of 1,1′-di-*n*-butyl-3,3′-methylenediimidazolium diiodide (0.045 g, 0.087 mmol), Ag_2O (0.04 g, 0.17 mmol), and the dichloro-bridged cyclometalated iridium complex $[(dfppy)_2Ir(\mu\text{-}Cl)]_2$ (0.05 g, 0.04 mmol) in 2-ethoxyethanol (10 mL) was heated to reflux for 12 h in the dark. After cooling to room temperature, the solution was filtered through a sintered-glass frit and an excess (10 equiv) of NH_4PF_6(in 20 mL H_2O) was added to induce precipitation. The yellow precipitate was collected by filtration, washed with H_2O, and then dried under vacuum. The solid was separated using silica gel column chromatography (CH_2Cl_2:MeCN = 9:1), giving a light-yellow complex **2a** (0.056 g, 0.057 mmol, 79% yield).

Spectra. ^{1}H NMR (300 MHz, acetone): δ 8.51 (dd, J = 0.8 and 5.9, 1H), 8.48−8.40 (m, 1H), 8.11 (ddd, J = 0.9, 7.5, and 8.3, 1H), 7.61 (d, J = 2.0, 1H), 7.39−7.29 (m, 2H), 6.60 (ddd, J = 2.4, 9.2, and 12.9, 1H), 6.35 (s, 1H), 5.87 (dd, J = 2.4 and 8.5, 1H), 3.59−3.33 (m, 2H), 1.29−1.09 (m, 1H), 0.94−0.74 (m, 2H), 0.65 (t, J = 7.2, 3H), 0.52−0.30 (m, 1H). $^{19}F\{^1H\}$ NMR (282 MHz, acetone): δ −71.16 (3F), −73.66 (3F), −109.20 (2F), −110.38 (2F). ^{13}C NMR (101 MHz, DMSO): δ 168.18, 164.45, 163.56, 162.24, 161.14, 159.53, 159.28, 153.85, 138.90, 128.18, 124.55, 123.53, 123.14, 122.98, 112.24, 97.64, 62.02, 48.61, 32.78, 19.42, 13.68. HRMS. Found: m/z 833.2576 ($[M - PF_6]^+$). Anal. Calcd for $C_{37}H_{36}F_{10}IrN_6P$: C, 45.44; H, 3.71; N, 8.59. Found: C, 45.04; H, 3.62; N, 8.41.

Preparation of Bis[2-(4,6-difluorophenyl)pyridinato-N,C^2]-iridium(III) [1,1′-Di-*n*-butyl-3,3′-methylenediimidazoline-2,2′-diylidene]tetrafluoroborate (2b). A mixture of 1,1′-di-*n*-butyl-3,3′-methylenediimidazolium diiodide (0.045 g, 0.087 mmol), Ag_2O (0.04 g, 0.17 mmol), and the dichloro-bridged cyclometalated iridium complex $[(dfppy)_2Ir(\mu\text{-}Cl)]_2$ (0.05 g, 0.04 mmol) in 2-ethoxyethanol (10 mL) was heated to reflux for 12 h in the dark. After cooling to room temperature, the solution was filtered through a sintered-glass frit and an excess (10 equiv) of $NaBF_4$ (in 20 mL of H_2O) was added to induce precipitation. The yellow precipitate was collected by filtration, washed with H_2O, and then dried under vacuum. The solid was separated using silica gel column chromatography (CH_2Cl_2:MeCN = 9:1), giving a light-yellow complex **2b** (0.055 g, 0.059 mmol, 74% yield).

Spectra. ^{1}H NMR (300 MHz, acetone): δ 8.52 (dd, J=0.8 and 5.9, 1H), 8.43 (d, J = 8.7, 1H), 8.11 (dd, J=7.7 and 8.5, 1H), 7.64 (d, J = 2.0, 1H), 7.39−7.26 (m, 2H), 6.60 (ddd, J = 2.4, 9.2, and 12.9, 1H), 6.34 (s, 1H), 5.87 (dd, J = 2.4 and 8.5, 1H), 3.58−3.35 (m, 2H), 1.19 (td, J = 5.8 and 10.9, 1H), 0.96−0.72 (m, 2H), 0.65 (t, J=7.2, 3H), 0.53−0.27 (m, 1H). $^{19}F\{^1H\}$ NMR (282 MHz, acetone): δ −109.27 (2F), −110.44 (2F), −151.04 (4F). ^{13}C NMR (101 MHz, DMSO): δ 168.16, 164.36, 163.55, 162.30, 160.85, 159.64, 159.13, 153.76, 138.92, 128.06, 124.20, 123.52, 122.80, 122.44, 112.12, 97.48, 61.77, 48.55, 32.63, 19.27, 13.19. HRMS. Found: m/z 833.2558 ($[M - BF_4]^+$). Anal. Calcd for $C_{37}H_{36}BF_8IrN_6$: C, 48.32; H, 3.95; N, 9.14. Found: C, 48.01; H, 4.03; N, 9.05.

Photophysics. Absorption spectra were measured on a Varian Cary 5000 double-beam UV−vis−near-IR spectrometer and baseline-corrected. Steady-state emission spectra were recorded on a Horiba Jobin-Yvon IBH FL-322 Fluorolog 3 spectrometer equipped with a 450 W xenon arc lamp, double-grating excitation, and emission monochromators (2.1 nm mm of dispersion^{-1}; 1200 grooves mm^{-1}) and a Hamamatsu R928 photomultiplier tube or a TBX-4-X single-photon-counting detector. Emission and excitation spectra were corrected for source intensity (lamp and grating) and emission spectral response (detector and grating) by standard correction curves. Time-resolved measurements were performed using the time-correlated single-photon-counting option on the Fluorolog 3. NanoLEDs (295, 402, and 431 nm; fwhm < 750 ps) with repetition rates between 10 kHz and 1 MHz were used to excite the sample. The excitation sources were mounted directly on the sample chamber at 90° to a double-grating emission monochromator (2.1 nm mm of dispersion^{-1}; 1200 grooves mm^{-1}) and collected by a TBX-4-X single-photon-counting detector. The photons collected at the detector are correlated by a time-to-amplitude converter to the excitation pulse. Signals were collected using an IBH DataStation Hub photon-counting module and data analysis was performed using the commercially available DAS6 software (Horiba Jobin-Yvon IBH). The quality of the fit was assessed by minimizing the reduced χ^2 function and visual inspection of the weighted residuals. The quantum yield measurements were performed in a deaerated dichloromethane (DCM) solution at 300 nm of excitation wavelength using the absolute quantum yield measurement system from Hamamatsu, model C9920-01.

X-ray Crystallography. Data sets were collected with a Nonius Kappa CCD diffractometer, equipped with a rotating-anode generator. Programs used: data collection, *COLLECT*;[14]data reduction, *Denzo-SMN*;[15] absorption correction, *SORTAV*[16,17] and *Denzo*;[18] structure solution, *SHELXS-97*;[19] structure refinement, *SHELXL-97*;[20] graphics, *SCHAKAL*.[21] The crystallographic refinement parameters of complexes **1a** and **2a** are summarized in Table S1 in the Supporting Information, and Figure S1 in the Supporting Information shows the crystal structure of complex **1a**.

Cyclic Voltammetry (CV). CV was performed using a CH Instrument workstation, which consists of a CH750 potentiostat and software. The working and counter electrodes were a platinum disk and a platinum wire, respectively, whereas a silver wire was used as the pseudoreference electrode. All glassware was dried prior to use. The dry electrolyte tetrabutylammonium perchlorate ($>99.0\%$ purity) was used after recrystallization. The analyte and ferrocene ($FeCp_2$) used as the reference were dried and degassed at high temperature and at reduced pressure in a Schlenk flask in order to eliminate any moisture and oxygen. The flask was then evacuated and filled three times with a nitrogen flow. Acetonitrile freshly distilled from P_2O_5 was added via syringe directly into the sealed Schlenk flask; the solution was sonicated if necessary and then degassed for 10 min with a gentle stream of nitrogen. The degassed solution was injected into the electrochemical cell, and after the introduction of electrodes, measurements were done under a nitrogen atmosphere.

Computational Method

The ground-state geometry of complexes **1a** and **2a** has been optimized at the density functional theory (DFT) level, starting from the X-ray structures and from the measured distance between the Ir center and the P atom of the PF_6^- counterion. The chosen exchange correlation functional is the widely used B3LYP[22] in view of its good compromise between accuracy and computational cost; the basis set for the description of the electrons of nonmetallic atoms is 6-31G**,[23] while the LANL2DZ basis set has been used for Ir.[24] Characterization of the nature of the lowest-lying singlet and triplet excited states relies on time-dependent DFT (TD-DFT) calculations performed on the basis of the ground-state geometry, using the same functional and basis set. This choice is motivated by previous works showing the adequacy of this approach to describe the electronic and optical properties of iridium complexes[25] and of other complexes.[26] Note that these calculations neglect intersystem crossing processes mixing states of the singlet and triplet manifold. All calculations were performed with the *Gaussian03* code.[27]

Fabrication of Light-Emitting Devices. All devices had an active area of 4 mm^2 and were fabricated by spin-coating on indium−tin oxide-coated glass substrates. The device structure consists of 100 nm poly(3,4-ethylenedioxythiophene):poly(styrenesulfonate) (PEDOT:PSS) and 70 nm of an emitting layer composed of iTMC blended with tetrabutylammonium trifluoromethanesulfonate (TBAOTf) as the ionic conductor. PEDOT:PSS (Clevios AI4083) was supplied by H. C. Starck, and TBAOTf was from Sigma Aldrich. The emitting-layer solution was prepared in the following way: 10 mg of the iTMC material together with the ionic conductor was diluted in 1 mL of acetonitrile in a mole ratio 1:1. Before spin coating, the solution was filtered using a 0.1 μm poly(tetrafluoroethylene) filter. The wet film was baked for 2 h at 80 °C in a vacuum oven. Finally, a 150−200-nm-thick aluminum cathode was evaporated on top, followed by an encapsulation to protect the organic layers from oxygen and water. All electrical characterizations of the LEECs were performed using a power sourcemeter E3646A from Agilent Technologies. The resulting light output was detected by photodiodes. The induced current through the device and through the photodiodes were measured by current meters from National Instruments (NI9219). The current compliance for the device current was set to 40 mV. Using a spectral camera (PR650), the photodiode current was calibrated and the EL spectra of the different LEEC devices were detected in the visible range between 380 and 780 nm.

Result and Discussion

Synthesis and X-ray Structure Characterization. A synthetic pathway leading to the desired iridium(III) complexes is depicted in Scheme 1. The targeted complexes were synthesized using the iridium dimer complex $[(dfppy)_2Ir(\mu\text{-}Cl)]_2$ with a stoichiometric amount of methyl- or *n*-butyl-substituted bisimidazolium salts and Ag_2O in 2-ethoxyethanol, to promote the chloride removal, followed by the replacement of Cl^- with PF_6^- or BF_4^-. The synthesized complexes containing the *n*-butyl group as a substituent of the carbene ligand are useful to increase the solubility of the complex in common organic solvents.

After purification and recrystallization of the complexes, detailed characterizations were carried out using high-resolution mass spectrometry, ^1H, ^{13}C, and ^{19}F NMR spectroscopy, and elemental analysis (see the Experimental Section for details).

Crystals of **1a** and **2a** suitable for X-ray diffraction analysis were obtained by the slow evaporation of diethyl ether into an acetonitrile solution. Table 1 reports selected bond lengths and angles for the structures. As depicted in Figure 1, complex **2a** exhibits a distorted octahedral geometry around the Ir atom coordinated to two

---

(14) *COLLECT*; Nonius, B. V.: Delft, The Netherlands, 1998.

(15) Otwinowski, Z.; Minor, W. *Macromolecular Crystallography*; Academic Press Inc.: San Diego, 1997; Vol. *276*, Part A, p 307.

(16) Blessing, R. H. *Acta Crystallogr., Sect. A* **1995**, *51*, 33.

(17) Blessing, R. H. *J. Appl. Crystallogr.* **1997**, *30*, 421.

(18) Otwinowski, Z.; Borek, D.; Majewski, W.; Minor, W. *Acta Crystallogr., Sect. A* **2003**, *59*, 228.

(19) Sheldrick, G. M. *Acta Crystallogr., Sect. A* **1990**, *46*, 467.

(20) Sheldrick, G. M. *SHELXL-97*; Universität Göttingen: Göttingen, Germany, 1997.

(21) Keller, E. *SCHAKAL*; Universität Freiburg: Freiburg, Germany, 1997.

(22) (a) Lee, C. T.; Yang, W. T.; Parr, R. G. *Phys. Rev. B* **1988**, *37*, 785. (b) Becke, A. D. *J. Chem. Phys.* **1993**, *98*, 5648.

(23) Curtiss, L. A.; Redfern, P. C.; Raghavachari, K.; Pople, J. A. *J. Chem. Phys.* **2001**, *114*, 108.

(24) Chiodo, S.; Russo, N.; Sicilia, E. *J. Chem. Phys.* **2006**, *125*, 104107.

(25) Avilov, I.; Minoofar, P.; Cornil, J.; De Cola, L. *J. Am. Chem. Soc.* **2007**, *129*, 8247.

(26) Vlcek, A.; Zalis, S. *Coord. Chem. Rev.* **2007**, *251*, 258.

(27) Frisch, M. J.; Trucks, G. W.; Schlegel, H. B.; Scuseria, G. E.; Robb, M. A.; Cheeseman, J. R.; Montgomery, J. A., Jr.; Vreven, T.; Kudin, K. N.; Burant, J. C.; Millam, J. M.; Iyengar, S. S.; Tomasi, J.; Barone, V.; Mennucci, B.; Cossi, M.; Scalmani, G.; Rega, N.; Petersson, G. A.; Nakatsuji, H.; Hada, M.; Ehara, M.; Toyota, K.; Fukuda, R.; Hasegawa, J.; Ishida, M.; Nakajima, T.; Honda, Y.; Kitao, O.; Nakai, H.; Klene, M.; Li, X.; Knox, J. E.; Hratchian, H. P.; Cross, J. B.; Bakken, V.; Adamo, C.; Jaramillo, J.; Gomperts, R.; Stratmann, R. E.; Yazyev, O.; Austin, A. J.; Cammi, R.; Pomelli, C.; Ochterski, J. W.; Ayala, P. Y.; Morokuma, K.; Voth, G. A.; Salvador, P.; Dannenberg, J. J.; Zakrzewski, V. G.; Dapprich, S.; Daniels, A. D.; Strain, M. C.; Farkas, O.; Malick, D. K.; Rabuck, A. D.; Raghavachari, K.; Foresman, J. B.; Ortiz, J. V.; Cui, Q.; Baboul, A. G.; Clifford, S.; Cioslowski, J.; Stefanov, B. B.; Liu, G.; Liashenko, A.; Piskorz, P.; Komaromi, I.; Martin, R. L.; Fox, D. J.; Keith, T.; Al-Laham, M. A.; Peng, C. Y.; Nanayakkara, A.; Challacombe, M.; Gill, P. M. W.; Johnson, B.; Chen, W.; Wong, M. W.; Gonzalez, C.; Pople, J. A. *Gaussian 03*, revision C.02; Gaussian, Inc.: Wallingford, CT, 2004.

Scheme 1. Synthetic Pathways and Chemical Structures and Abbreviations of the Investigated Complexes

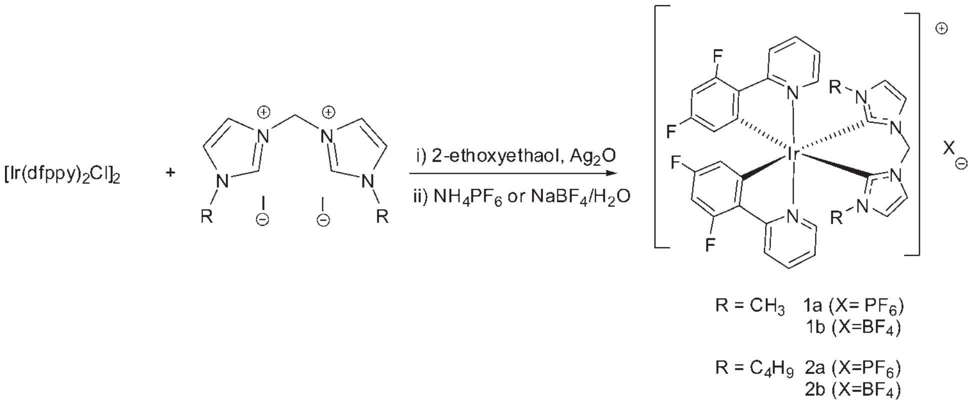

Table 1. Selected Bond Length (Å) and Angles (deg) for Complexes **1a** and **2a**

	Complex **1a**·PF_6·CH_3CN		
Ir−$C_{carbene}$(1)	2.112(5)	Ir−$C_{carbene}$(11)	2.114(5)
Ir−N(21)	2.053(4)	Ir−C(32)	2.063(4)
Ir−N(41)	2.052(4)	Ir−C(52)	2.043(4)
C(1)−Ir−C(32)	173.22(17)	C(52)−Ir−C(11)	172.74(18)
N(21)−Ir−N(41)	169.39(16)	C(32)−Ir−N(21)	79.19(17)
C(52)−Ir−N(41)	79.65(17)	C(1)−Ir−C(11)	85.82(18)
	Complex **2a**·PF_6·CH_3CN		
Ir−$C_{carbene}$(2)	2.120(1)	Ir−$C_{carbene}$(12)	2.104(1)
Ir−N(21)	2.055(1)	Ir−C(32)	2.054(1)
Ir−N(41)	2.072(1)	Ir−C(52)	2.054(1)
C(2)−Ir−C(32)	173.58(14)	C(52)−Ir−C(12)	174.94(12)
N(21)−Ir−N(41)	170.77(12)	C(32)−Ir−N(21)	80.00(14)
C(52)−Ir−N(41)	79.20(14)	C(2)−Ir−C(12)	85.28(15)

cyclometalated dfppy ligands and one symmetrical biscarbene ligand. The dfppy ligands adopt a mutually eclipsed configuration, with the N atoms N(21) and N(41) residing at the trans locations with distances Ir−N(21) = 2.055(1) Å and Ir−N(41) = 2.072(1) Å. The substituted phenyl groups are arranged cis to each other with the distances Ir−C(32) = 2.054(1) Å and Ir−C(52) = 2.054(1) Å. Moreover, the overall structural arrangement is similar when compared to several previously reported examples.[28] The pertinent bond angles and distances around iridium are identical within their estimated standard deviation, indicating that the peripheral methyl and *n*-butyl substituents have no significant stereoelectronic effects on the metal center. The carbene bite angles C(1)−Ir−C(11) (**1a**) and C(2)−Ir−C(12) (**2a**) of 85.82(18)° and 85.28(15)° are very appropriate for octahedral coordination. To the best of our knowledge, this is the first structure of a bisimidazolium carbene ligand bound to a phenylpyridine complex.

We have first validated our theoretical approach by comparing the representative distance and bond angle of the DFT-optimized geometries to the corresponding experimental values. This information is included in Table S2 in the Supporting Information.

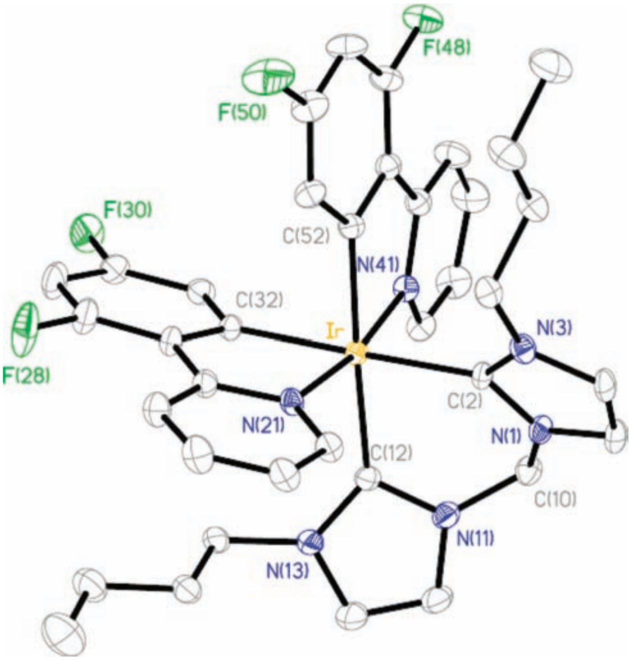

Figure 1. ORTEP diagram of **2a** with thermal ellipsoids shown at the 30% probability level. The CH_3CN solvent molecules, counteranions (PF_6^-), and H atoms are omitted for clarity.

The calculated and experimental geometric parameters are in very good agreement, with differences systematically below 3%. The best match is found for the Ir−C(dfppy) distance and for the angle values, while the Ir−C(carbene) distances differ typically by 2−3% compared to the experimental values. This agreement ensures a proper description of the nature of the lowest excited states, provided that the complex keeps a similar geometry in solution.

There is a larger discrepancy when comparing the distance between the Ir atom in the complex and the P atom in the counterion (Ir−P = 7.137 Å in the X-ray structure versus Ir−P = 6.284 Å at the theoretical level; see Figure 2). This can be intuitively understood by the fact that the location of the counterion is more flexible in the gas phase (or in solution) compared to the solid state. The geometric parameters are found to be weakly affected when the counterion is not included, thus showing the weak impact of the electrostatic interactions on the

---

(28) (a) Coppo, P.; Plummer, E. A.; De Cola, L. *Chem. Commun.* **2004**, 1774. (b) Orselli, E.; Kottas, G. S.; Konradsson, A. E.; Coppo, P.; Fröhlich, R.; De Cola, L.; Van Dijken, A.; Büchel, M.; Börner, H. *Inorg. Chem.* **2007**, *46*, 11082. (c) Orselli, E.; Albuquerque, R. Q.; Michel Fransen, P.; Fröhlich, R.; Janssenc, H. M.; De Cola, L. *J. Mater. Chem.* **2008**, *18*, 4579.

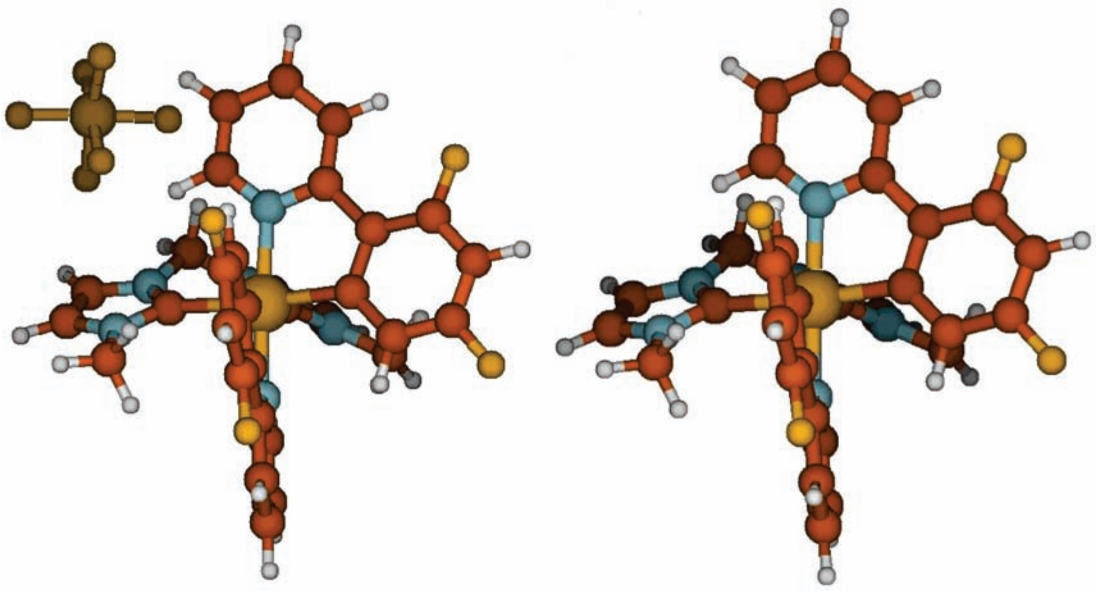

Figure 2. Calculated molecular geometries of complex **1a** with (left) and without (right) the counterion.

molecular geometry. On the other hand, the counterion has a strong impact on the electronic structure of the complexes; this is illustrated in Table S3 in the Supporting Information, showing the contribution of the different fragments (Ir, carbene ligand, dfppy1 and dfppy2, and counterion) to the frontier electronic levels of complex **1a** as well as the energies of these levels from calculations performed with and without the counterion. Similar trends are observed for complex **2a**. These results indicate that the counterion does not participate in the description of the frontier electronic levels; however, the electrostatic interactions induced by the counterion are found to significantly shift the energies of the one-electron levels, to modulate for some their fragment contributions, and to break the symmetry of the orbitals localized on the individual ligands (when the counterion is not positioned symmetrically with respect to the ligand). The electronic structure of the complexes and their optical properties are discussed hereafter on the basis of the optimized ground-state geometry in the presence of the counterion. The most stable geometry of the system has first been determined by running geometry optimizations from starting geometries featuring different locations of the counterion.

Electronic Structure. We have first examined the nature of the frontier electronic levels that will be predominantly involved in the lowest excited states of the complexes, by analyzing for each electronic level the contribution of the different fragments. Table 2 collects the energies of the frontier electronic levels of complexes **1a** and **2a** as well as the contribution of the different fragments.

Table 2. Energies and Contribution (in percent) of the Different Fragments for the Frontier Electronic Levels Ranging from HOMO−5 to LUMO+5, for Complexes **1a** (Left) and **2a** (Right), Which Are Referred to as H−5 and L+5 in the Table

FO	energy	Ir	methyl	dfppy1	dfppy2	energy	Ir	butyl	dfppy1	dfppy2
H−5	−6.72	4	16	34	46	−6.66	5	13	14	67
H−4	−6.61	42	15	23	19	−6.49	6	19	30	45
H−3	−6.50	20	15	23	41	−6.29	45	21	14	19
H−2	−6.45	45	21	9	24	−6.23	15	14	48	22
H−1	−6.30	16	9	60	15	−6.20	42	26	24	8
H	**−5.95**	**43**	**11**	**31**	**16**	**−5.83**	**43**	**13**	**32**	**12**
L	**−2.06**	**5**	**3**	**3**	**90**	**−1.95**	**4**	**5**	**2**	**88**
L+1	−1.59	5	5	87	3	−1.55	4	4	86	5
L+2	−1.55	4	5	2	89	−1.41	3	4	4	89
L+3	−0.96	5	5	88	3	−0.88	3	6	86	4
L+4	−0.53	14	69	6	11	−0.28	18	46	10	26
L+5	−0.19	7	46	41	6	−0.06	9	27	4	59

The contributions of the different fragments in the HOMO and LUMO are similar for both complexes. The HOMO level has a strong weight on Ir, while the LUMO is essentially localized on dfppy2. However, the occupied levels become already different for the HOMO−1 level, which has its largest contribution from Ir in **2a** and from dfppy1 in **1a**. Actually, the HOMO−1 level of **2a** appears to be very similar to the HOMO−2 of **1a**, thus pointing to changes in the ordering of the states between the two complexes as expected from their small energy separation. This one-to-one correspondence is extended down to the HOMO−5 orbital. On the other hand, the nature of the lowest unoccupied levels is very similar in the two complexes up to the LUMO+4 level. Next we go deeper into the analysis of the electronic structure of complex **1a**. The electronic structure and shape of the frontier electronic levels of this complex is graphically displayed in Figure 3.

The contribution of the carbene ligand is small for the orbitals ranging from HOMO−5 to LUMO+3 while reaching typical values larger than 35% in deeper levels. The two phenylpyridine moieties are alternatively the most contributing ligand going from LUMO to LUMO+3. These two ligands are thus expected to be strongly involved in the description of the low-lying excited states. Moreover, they contribute to most of the orbitals by more than 20% so that many excited states should be described by a mixture of different transition-metal characters. In both complexes, the largest electronic density in the HOMO is supported by the phenyl ring of dfppy, while the LUMO is mostly centered on the pyridine ring, as expected from the larger electronegativity of the N atom. When the size of the alkyl chains increased,

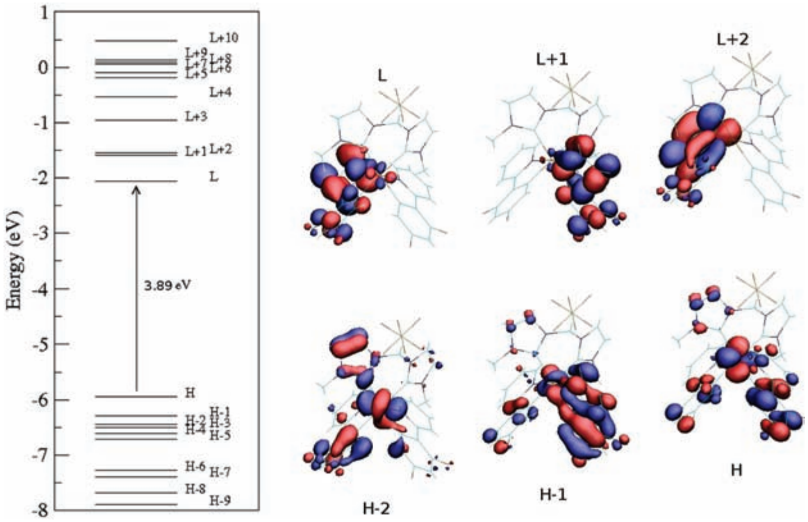

Figure 3. Electronic structure and shape of the frontier electronic levels from HOMO−2 to LUMO+2, referred to as H−2 and L−2, respectively, of complex **1a**.

going from **1a** to **2a**, the order of the highest occupied levels is reversed, while the other electronic levels experience an energy shift; on the other hand, the electronic bandgap is found to be very similar for both complexes.

Photophysical Properties. Figure 4 shows the UV−vis absorption and emission spectra of complexes **1** and **2** in CH_2Cl_2 solutions. In general, the dominant absorption band in the spectral region ≤300 nm is attributed to the spin-allowed $^1\pi\pi^*$ transition characteristic of the ligands. The structureless band at ~300−360 nm for **1** and **2** is likely to result from the combination of a substituted phenyl-to-pyridine interligand $\pi\pi^*$ transition (LLCT) with Ir(d_π) to a phenylpyridyl ligand transition (MLCT) in the singlet manifold. The lowest-lying bands that appear in the region >360 nm are assigned to singlet and triplet MLCT transitions, which, however, have a strong $\pi\pi^*$ transition character. In this context, we have calculated the nature of lowest singlet excited states at the TD-DFT level strongly coupled to the singlet ground state to assist the interpretation of the experimental spectra.

Table 3 reports the calculated energies of the excited states with the largest oscillator strengths together with the nature of the dominant one-electron transition. The theoretical results reproduce very well the three energy ranges observed in the experimental spectra, yielding the most intense band located around 250 nm, the second one around 300 nm, and a less intense peak at 340 nm for both complexes **1a** and **2a**. Note that the lowest excited state mostly described by a HOMO-to-LUMO transition (94%) is calculated at 392 nm; however, this state cannot be isolated in the experimental spectrum because of its very small oscillator strength and is most likely merged with the tail of the lowest absorption band.

Even though there is a different ordering of the highest occupied levels between complexes **1a** and **2a** (see Table 2), we find a consistency in the electronic character of the states involved in each of the three energy regions (see Table 3). Note that state 9 in complex **2a** lies in between bands 2 and 3 but has been associated with band 2 because of the similarity of the electronic character. We describe hereafter in detail the nature of the excited states in complex **1a**, pointing to the differences observed for **2a**.

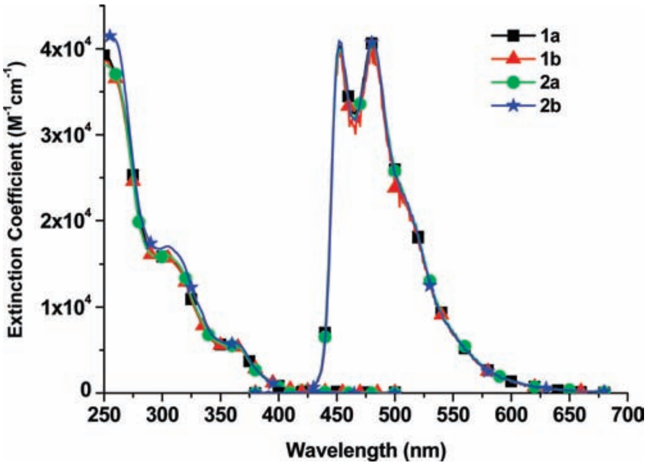

Figure 4. Absorption and PL spectra in DCM solution at room temperature.

Table 3 shows that the virtual orbitals involved in the dominant one-electron transitions are the LUMO, LUMO+1, and LUMO+2 for complex **1a** (LUMO and LUMO+1 for complex **2a**). The orbitals are strongly localized (more than 87%) on the dfppy ligands, thus confirming the key role played by these ligands. In the energy region around 250 nm (band 3), we find states with a dominant IL character involving either dfppy1 or dfppy2, as predicted, but also states with dominant LMCT and LLCT contributions in complex **1a**. For the states in the energy region around 300 nm (band 2), the largest contributing character in the dominant transition is intraligand (IL)-centered on dfppy1 for state 9 and on dfppy2 for state 15 in **1a**. Note that, for complex **2a**, there is also an important LLCT character in state 16, thus explaining the lower oscillator strength compared to state 11, exhibiting a dominant IL character. In the energy range between 305 and 340 nm (band 1), there is MLCT character involving dfppy1 in state 3, while the most important character in state 6 is IL targeted to dfppy2. Finally the dominant character of the lowest excited state (band 1′) around 390 nm is linked to a charge transfer from Ir to dfppy2. However, there is also a small IL

Table 3. Characterization of the Most Optically Coupled Lowest Singlet Excited States (ES)[a]

1a	ES	Occc	Vir	eV/nm	*f*	%	character
band 1′	1	H	L	3.16/393	0.01	94	MLCT (40%), LLCT (30%)
band 1	3	H	L+1	3.63/341	0.03	89	MLCT
	6	H−3	L	3.81/325	0.06	25	IL
band 2	9	H−1	L+1	4.09/302	0.05	50	IL
	15	H−3	L+2	4.33/286	0.05	36	IL
band 3	22	H−6	L	4.69/264	0.17	37	LMCT (30%), LLCT (23%)
	24	H−1	L+3	4.79/259	0.10	48	IL
2a	ES	Occ	Vir	eV/nm	*f*	%	character
band 1′	1	H	L	3.16/392	0.01	94	MLCT(40%), LLCT(30%)
band 1	4	H−3	L	3.62/343	0.03	73	MLCT
	7	H−4	L	3.92/316	0.03	77	IL (40%), LLCT (30%)
	9	H−3	L+1	4.03/307	0.05	52	MLCT
band 2	11	H−2	L+1	4.15/299	0.08	40	IL
	16	H−4	L+1	4.37/284	0.05	59	LLCT (40%), IL (30%)
band 3	22	H−5	L+2	4.69/264	0.07	45	IL
	30	H-2	L+3	4.95/251	0.12	28	IL

[a] We provide the nature of the dominant one-electron transition from a given occupied (Occ) to unoccupied (Vir) level including the contribution in percents as well as the oscillator strength (*f*) and energy of the states both in electronvolts and nanometers. The second most important character has been included only when its weight is larger than two-thirds of the most important one. The weight of the characters in percent is included in parentheses.

character that promotes a significant value for the transition dipole moment because MLCT and LLCT transitions alone would give rise to very low values. We have further compared the relative intensities of bands 1−3 by plotting in Figure 5 the simulated spectra of the two complexes.[29] The calculated relative intensities of the three bands are consistent with the experimental spectra (40, 15, and 5 × 10^3 M^{-1} cm^{-1} for bands 3, 2, and 1 to be compared with the calculated values of 30, 18, and 10 × 10^3 M^{-1} cm^{-1} for complex **1a** and 25, 20, and 6 × 10^3 M^{-1} cm^{-1} for complex **2a**).

Complexes **1** and **2** exhibit an intense blue emission with a 0−0 transition at ∼452 nm in a degassed CH_2Cl_2 solution and thin film (see Figure 6 and Table 4). All complexes show vibronically structured emission spectra at room temperature, indicating that the emissive excited states have a pronounced LC $\pi\pi^*$ character in addition to MLCT character. Moreover, upon cooling of the solution to 77 K, the emission spectra of the complexes are much more structured and blue-shifted (see Figures S2−S5 in the Supporting Information). The results unambiguously indicate that the lowest-lying triplet excited state is a MLCT, as supported by the shift in energy of the emission upon cooling, with a pronounced $\pi\pi^*$ character. The spectral profile is reminiscent of other iridium(III) complexes having a dfppy cyclometalated chelate and is comparable to that of cationic "blue-emitting" iridium(III) complexes with strongly π-accepting ligands.[7d,10a]

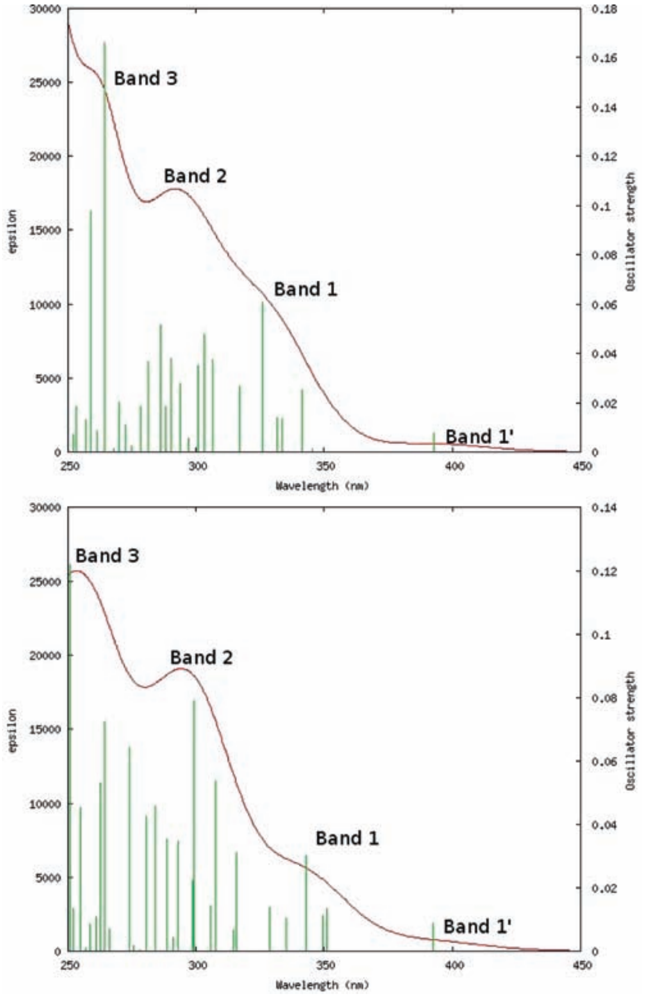

Figure 5. TD-DFT simulated absorption spectra of complexes **1a** (up) and **2a** (down) using a full width at half-maximum of 3000 cm^{-1}. The vertical bars correspond to the individual excited states.

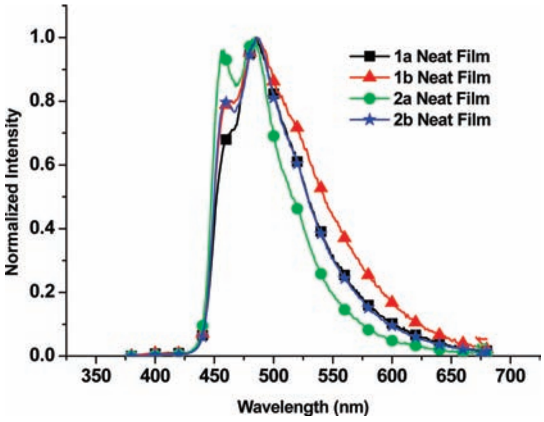

Figure 6. Emission spectra of iridium complexes in a neat film.

Table 5 describes the nature of the lowest triplet excited state of complexes **1a** and **2a** provided by TD-DFT calculations from the ground-state geometry in the absence of spin−orbit coupling. The dominant character of the emitting state is MLCT, with some admixture of LLCT and IL for **1a** and mostly MLCT for **2a**. The energy separation between the lowest singlet and triplet excited states is estimated by theory to be 0.32 and 0.30 eV for complexes **1a** and **2a**, respectively. This value is smaller than 0.70 eV estimated from the experimental data by subtracting the energy of the 0−0 peak of the lowest

---

(29) O'Boyle, N. M.; Tenderholt, A. L.; Langner, K. M. *J. Comput. Chem.* **2008**, *29*, 839.

Table 4. Photophysical and Electrochemical Data of Iridium Complexes

	em λ/nm^a, Φ_{sol}^{d}	λ_{film}/nm^b, Φ_{film}^{d}	λ_{film}/nm^c, Φ_{film}^{d}	τ_{obs}/μs	k_r (10^5 s^{-1})	k_{nr} (10^5 s^{-1})	E_{ox}/V^e	E_{re}/V^e
1a·PF_6	452, 482 [0.20]	460, 484 [0.02]	457, 484 [0.07]	2.08	0.96	3.8	0.99	−2.32, −2.67
1b·BF_4	452, 480 [0.30]	458, 484 [0.03]	457, 484 [0.07]	2.33	1.28	3.0	0.97	−2.39, −2.67
2a·PF_6	452, 482 [0.26]	458, 484 [0.06]	455, 483 [0.14]	2.21	1.18	3.35	1.04	−2.38, −2.67
2b·BF_4	452, 480 [0.35]	458, 484 [0.06]	454, 482 [0.13]	2.35	1.49	2.77	1.05	−2.37, −2.67

[a] Degassed CH_2Cl_2 solution (298 K). [b] Neat film. [c] Film containing TBAOTf (1:1 molar ratio). [d] PL quantum yields were determined with a calibrated integrating sphere system. [e] Electrochemical data versus Fc^+/Fc (Fc is ferrocene) were collected in MeCN.

Table 5. Characterization of the First Triplet Excited State at the TD-DFT Level in the Absence of Spin−Orbit Coupling[a]

	Occ	Vir	eV/nm	%	character	S_1-T_1/eV
1a	H	L	2.84/436	46	MLCT (43%), LLCT (31%)	0.32
	H−3	L		15	IL	
2a	H	L	2.86/434	34	MLCT (43%), LLCT (32%),	0.30
	H−3	L		21	MLCT	

[a] We provide the same parameters as those in Table 3, together with the energy separation between S_1 and T_1, as obtained from the ground-state geometry.

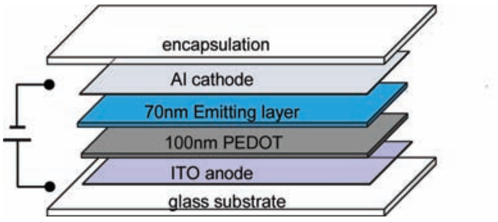

Figure 7. Schematic view of the device structure.

emission band (~2.74 eV) from the energy of the lowest intense absorption band (around ~3.44 eV) because the latter does not correspond to the lowest excited state. Moreover, the theoretical value is expected to be larger when accounting for the lattice relaxation effects in the triplet emitting state.

The absolute emission quantum yields of **1** and **2** measured by an integrating sphere are in the range of $\Phi = 0.20-0.35$ in degassed CH_2Cl_2 (see Table 4). We can observe that for complexes containing the BF_4^- counterion the quantum yield is slightly higher than that of the corresponding complexes having the PF_6^- counterion. We have also measured the emission quantum yields of neat films and films with TBAOTf. The data show that the complexes with long *n*-butyl chains possess emission quantum yields double those complexes containing short methyl chains. This effect could be due to the fact that the long *n*-butyl chain prevents stacking of the complexes, reducing the quenching effect in the film, by decreasing the triplet−triplet annihilation. The excited-state lifetimes of all of the complexes investigated are in the range of 2.08−2.35 μs. The excited-state lifetimes of complexes with the BF_4^- counterion are slightly longer than those of complexes with the PF_6^- ion. From the quantum yield (Φ) and the lifetime (τ) values, assuming a unitary intersystem crossing efficiency, the radiative and overall nonradiative rate constants k_r and k_{nr} were calculated for using the equations $k_r = \Phi/\tau$ and $k_{nr} = (1-\Phi)/\tau$ (see Table 4).[30]

Electrochemistry. The electrochemical behavior of these iridium metal complexes was investigated by CV using ferrocene as the internal standard. The results are summarized in Table 4. During the anodic scan in CH_3CN, all iridium metal complexes exhibited a reversible oxidation with potentials in the region of 0.97−1.05 V. Upon a switch to the cathodic sweep, two irreversible waves, with potentials ranging from −2.32 to −2.67 V, were detected. Since complexes **1** and **2** differ only by the nature of the terminal alkyl chain on the carbene ligand, their HOMO and LUMO levels, and hence their redox potentials, are expected to be similar. This is confirmed by the data in Table 2 showing that the HOMO is calculated at −5.95 and −5.83 eV for **1a** and **2a**, respectively, while the LUMO stands at −2.06 and −1.95 eV, respectively. Therefore, oxidation is expected to occur primarily on the iridium metal site, together with additional contributions from the cyclometalated dfppy ligands. On the other hand, the reduction process is concentrated on the pyridyl group of the dfppy chromophores.

EL Properties: LEEC Devices. A schematic representation of the device architecture is shown in Figure 7. To investigate the EL properties of the devices based on the different complex voltage sweeps, now referred to as voltage sweep mode (VSM), and to study the electric field stability range of the complexes as well as the time-dependent measurements at constant voltage, i.e., constant voltage mode (CVM), the luminance and current density were performed. In the case of VSM, the current density and luminance were measured starting at 0 V (at time 0), and every 60 s, the voltage was stepwise increased by 0.1 V until reaching 7.0 V. For CVM, a constant voltage of $U = 5.0$ V was applied and the luminance was scanned every 10 s. Each curve is an average over six devices. According to the first experiments, it turned out that the devices based on a neat film of complexes exhibited very long response times; the ionic conductor TBAOTf was added to the light-emitting layer to make the turn-on faster. The molar ratio of the iridium complex and TBAOTf was set to 1:1 because this yielded the best device performance.

In Figure 8, typical device characteristics in VSM (Figure 8a,b) and CVM (Figure 8c,d) for **1a**, **1b**, **2a**, and **2b** are shown. For all devices and for both operation modes, a curve progression with rising and falling slopes of the luminance was observed. For both modes, the rising slope can be referred to as decreasing injection barriers and a subsequent increase of the injected charge carriers into the device. In the case of VSM, such an injection enhancement is promoted by higher voltages due to a higher electrochemical potential difference between the anode and cathode. For the CVM, the increase in the current density and luminance is due to

---

(30) Kober, E. M.; Caspar, J. V.; Lumpkin, R. S.; Meyer, T. J. *J. Phys. Chem.* **1986**, *90*, 3722.

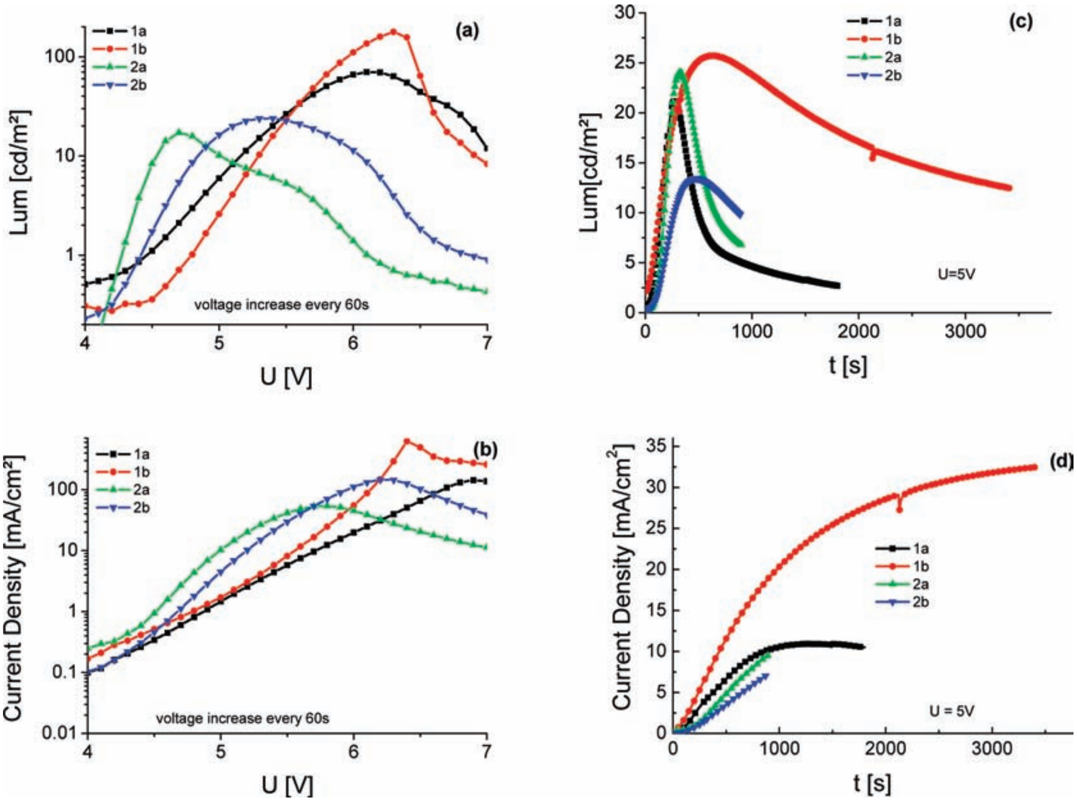

Figure 8. Voltage versus luminance (a) and voltage versus current density (b) curves under VSM. Time-dependent luminance (c) and time-dependent current density (d) curves under CVM.

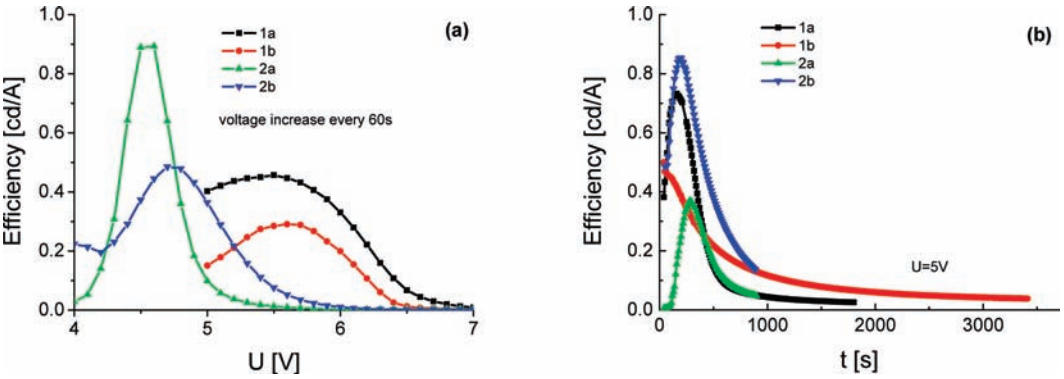

Figure 9. (a) Voltage versus current efficiency under VSM and (b) time-dependent current efficiency curves under CVM.

an increasing orientation of mobile ions along the external electrical field over time. The decay can be explained by device/complex instabilities at higher electric fields for VSM and time-dependent device/complex degradation for CVM.

As shown, the complexes including the short-methyl-chained biscarbene ligands (for **1a** and **1b**, Lum ≈ 70 and 180 cd m^{-2}) are more luminescent than the *n*-butyl long-chained ones (for **2a** and **2b**, both Lum ≈ 20 cd m^{-2}) in VSM. However, such high differences of the maximum luminance between **1a**/**1b** and **2a**/**2b** are only observed for higher voltages $U \geq 6.0$ V. In CVM, at $U = 5.0$ V, such diverse values are not significant because the maximum luminance of **2a** is comparable with that of **1a**/**1b** for example. The best results in CVM in terms of device stability were achieved for the short-chained carbene complex **1b** with the BF_4^- counterion. The time to reach the luminance maximum varies between 260 s (**1a**) and 620 s (**1b**). Interestingly, in both modes, the luminance maximum does not match the maximum of the current density. Such a mismatch between the current and light was also observed in former studies, e.g., for a $[Ir(ppy)_2(Hpbpy)][PF_6]$ complex reported by Bolink et al.[7d] In Figure 9, the current efficiency is depicted in VSM (Figure 9a) and CVM (Figure 9b). For both modes, a comparable curve progression with rising and falling slopes like those for the luminance characteristics was observed, whereas the efficiency maximum does not fit to the maximum of the luminance because of the mentioned mismatch between the luminance and current density. The characteristics of the devices based on the four iTMC complex strategies are summarized in Table 6.

Table 6. Summary of the Device Characteristics Based on Complexes **1a**–**2b**

complex	$t_{\max}{}^a$/min	$L_{\max}{}^b$/(cd m^{-2})	$L_{\max}{}^c$/(cd m^{-2})	eff.^{d}/(cd A^{-1})	eff.^{e}/(cd A^{-1})	$\lambda_{\max,\mathrm{EL}}{}^f$/nm	lifetime ^{g}/min	CIE(x,y)^h
1a	4.5	69.8	21.6	0.46	0.73	488	8.0	0.27, 0.43
1b	10.6	159.8	25.7	0.29	0.50	488	53.8	0.27, 0.43
2a	5.3	17.2	24.0	0.89	0.37	456, 488	9.8	0.20, 0.34
2b	7.8	23.8	13.4	0.49	0.85	456, 488	16.7	0.22, 0.38

[a] Time required to reach the maximal brightness in CVM. [b] Maximum brightness achieved in VSM. [c] Maximum brightness achieved at a constant bias voltage of 5.0 V (CVM). [d] Maximum current efficiency in VSM. [e] Maximum current efficiency in CVM. [f] EL peak wavelength measured at 5.5 V. [g] Time to decay to the half of the maximum luminance under a constant bias voltage of 5.0 V (CVM). [h] CIE evaluated from the EL spectra.

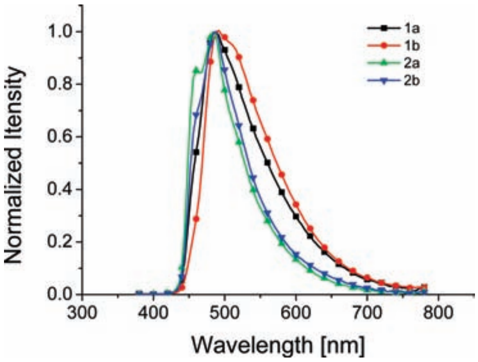

Figure 10. EL spectra for LEEC devices.

On the basis of the CV results shown in Table 4 with reversible oxidation from an anodic scan and irreversible reduction processes during the cathodic sweep of the complexes **1a**, **1b**,**2a**, and **2b** in solution, it is expected that hole transport is more pronounced and stable than electron transport in a LEEC configuration of these complexes. For a better charge balance and hence for a better LEEC performance, especially with higher luminance and efficiency values, blending the complexes with more electron-transporting materials could be a possible improvement.

In Figure 10, the EL emission spectra measured at a fixed voltage of 5.5 V are shown. In particular, complexes **2a** and **2b** exhibit a blue to blue-green emission with local maxima at wavelengths of about $\lambda_{\max} = 456$ and 488 nm. The CIE coordinate value of complex **2a** is (0.20, 0.34). The CIE value of the device incorporating **2a** and the ionic conductor indicate a substantially bluer emission than that for other blue-phosphorescent dopants.[10a]

The spectrum of complex **2a** is comparable to the thin-film PL spectra with a 1:1 molar ratio (Figure S4 in the Supporting Information). In contrast to that, the EL spectra of complexes **1a** and **1b** were red-shifted with a peak at 488 nm compared to the PL spectra in solution and thin film with a peak at about 452–458 nm (Figures S2–S5 in the Supporting Information). This similar red-shifted phenomenon for blue-emitting iridium LEECs has also been observed in a recent paper.[31] We believe that the longer alkyl chains in compound **2** prevent aggregation, which is responsible for the red shift of complex **1**. This finding could help in the design of the next generation of blue LEECs.

Conclusions

Four novel blue-emitting cationic iridium complexes have been synthesized and fully characterized. We have designed and used two types of biscarbenes as ancillary ligands differing in the length of the alkyl chain attached to the N atoms. We have prepared the corresponding cationic iridium complexes, isolating them using different counterions. Theoretical calculations address almost no difference between the two types of ancillary ligands for which the HOMO consists of a mixture between the Ir and dfppy species and the LUMO is mostly located on the other dfppy ligand. The importance of ^{3}LC character in the emissive states is confirmed by theoretical calculations. These iridium complexes exhibit efficient blue emission in solution and thin film. The LEEC devices made using the iridium(III) carbene type complex and a new ionic conductor (TBATOf) have short device turn-on times (a few seconds) and exhibit blue emission. Our molecular-design strategy based on using high-ligand-field carbene ligands suggests that the emission of iTMCs can be efficiently tuned to a blue or deep-blue region.

Acknowledgment. The authors thank Siemens AG, Corporate Technology, CT MM 1, and the European Community Seventh Framework Programme (FP7/2007-2013) under Grant 212311 of the ONE-P project for financial support. C.-H.Y. acknowledges the Humboldt Foundation for financial support. The work in Mons is also supported by the Belgian National Fund for Scientific Research (FNRS). This research used resources of the Interuniversity Scientific Computing Facility located at the University of Namur, Namur, Belgium, which is supported by the FRS-FNRS under Convention No. 2.4617.07. J.C. is a senior research associate of FNRS.

Supporting Information Available: X-ray crystallographic data file (CIF) for complexes **1a** and **2a**, ORTEP diagram of **1a**, crystal data and structure refinement parameters for complexes **1a** and **2a**, emission spectra of complexes **1a**, **1b**, **2a**, and **2b**, comparison between theory and experiment for the representative distances and bond angles in complexes **1a** and **2a**, and electronic structure of complex **1a** in absence or presence of the counterion. This material is available free of charge via the Internet at http://pubs.acs.org.

---

(31) (a) Bolink, H. J.; Cappelli, L.; Cheylan, S.; Coronado, E.; Costa, R. D.; Lardiés, N.; Nazeeruddin, M. K.; Ortí, E. *J. Mater. Chem.* **2007**, *17*, 5032. (b) Margapoti, E.; Shukla, V.; Valore, A.; Sharma, A.; Dragonetti, C.; Kitts, C. C.; Roberto, D.; Murgia, M.; Ugo, R.; Muccin, M. *J. Phys. Chem. C* **2009**, *113*, 12517.